UNIVERSITY OF BIRMINGHAM
University of Birmingham Research at Birmingham

Nonlinear modelling for structural damage assessments of reinforced and coated longitudinally coupled slab tracks

Li, Yang; Chen, Jinxie; Wang, Jianxin; Kaewunruen, Sakdirat

DOI:
10.1016/j.dibe.2023.100204

License:
Creative Commons: Attribution (CC BY)

Document Version
Publisher's PDF, also known as Version of record

Citation for published version (Harvard):
Li, Y, Chen, J, Wang, J & Kaewunruen, S 2023, 'Nonlinear modelling for structural damage assessments of reinforced and coated longitudinally coupled slab tracks', *Developments in the Built Environment*, vol. 15, 100204. https://doi.org/10.1016/j.dibe.2023.100204

Link to publication on Research at Birmingham portal

General rights
Unless a licence is specified above, all rights (including copyright and moral rights) in this document are retained by the authors and/or the copyright holders. The express permission of the copyright holder must be obtained for any use of this material other than for purposes permitted by law.

•Users may freely distribute the URL that is used to identify this publication.
•Users may download and/or print one copy of the publication from the University of Birmingham research portal for the purpose of private study or non-commercial research.
•User may use extracts from the document in line with the concept of 'fair dealing' under the Copyright, Designs and Patents Act 1988 (?)
•Users may not further distribute the material nor use it for the purposes of commercial gain.

Where a licence is displayed above, please note the terms and conditions of the licence govern your use of this document.

When citing, please reference the published version.

Take down policy
While the University of Birmingham exercises care and attention in making items available there are rare occasions when an item has been uploaded in error or has been deemed to be commercially or otherwise sensitive.

If you believe that this is the case for this document, please contact UBIRA@lists.bham.ac.uk providing details and we will remove access to the work immediately and investigate.

Download date: 02. May. 2024

Developments in the Built Environment 15 (2023) 100204

Contents lists available at ScienceDirect

Developments in the Built Environment

journal homepage: www.sciencedirect.com/journal/developments-in-the-built-environment

Nonlinear modelling for structural damage assessments of reinforced and coated longitudinally coupled slab tracks

Yang Li [a,b], Jinjie Chen [b,c], Jianxi Wang [b], Sakdirat Kaewunruen [a,*]

[a] Department of Civil Engineering, School of Engineering, The University of Birmingham, Birmingham, B15 2TT, UK
[b] State Key Laboratory of Mechanical Behavior and System Safety of Traffic Engineering Structures, Shijiazhuang Tiedao University, Shijiazhuang, 050043, China
[c] School of Transportation Engineering, Hebei University of Water Resources and Electric Engineering, Cangzhou, 061001, China

ARTICLE INFO

Keywords:
Longitudinally continuous slab track
Post-installed anchor
Solar reflective coating
Finite element model
Cohesive zone model
Bond-slip relationship

ABSTRACT

Interface debonding and slab end arching of the anchor-reinforced and coated longitudinally continuous slab tracks have been unprecedentedly investigated in this study. A novel finite element model of the longitudinally continuous slab track has been established by incorporating a tailored cohesive zone model to mimic nonlinear constitutive relationships. The new model has been validated by over 100 field measurement data. This paper is the first to assess the influences of the dual applications of anchors and coatings on the damages of the longitudinally continuous slab tracks, and to identify the effectiveness of different track maintenance methods in mitigating track damages. This study exhibits new findings: (1) In comparison with traditional tracks, the tracks constructed with anchors, coatings, and the combined use of both can reduce the maximum vertical relative displacement between the concrete slab and the mortar layer by 75%, 40%, and 85% respectively. (2) In comparison with 4 anchors, 6 or more anchors in each slab can help to prevent inner interface defects. However, an increase in anchor quantity above 6 anchors does not have a significant impact on the interface damage mitigation. (3) For the anchor-reinforced tracks, the organic coating outweighs the inorganic coating to improve interface damage mitigation.

1. Introduction

Highspeed railway (HSR) networks have been constructed around the world over recent decades in order to connect regional communities and major cities. HSRs are considered to be the most sustainable means among many other transport modes (Rungskunroch et al., 2021; Gesualdo and Penta, 2018; Yang et al., 2019; Kaewunruen et al., 2016). HSR tracks with a high standard of surface smoothness, structural integrity, and material durability are fundamental to the operational safety and reliability of HSR systems. However, certain track damages can be inevitable since railway tracks are not only subjected to repeated train loadings but also in most cases exposed to harsh environmental conditions (Matias and Ferreira, 2022). For instance, structural damages like interfacial gaps and slab end arching have been reportedly a pressing industry issue for highspeed rail longitudinally continuous tracks in China (Lu et al., 2022).

The longitudinally continuous slab track has been used in many HSR networks such as Beijing-Shanghai HSR, Beijing-Tianjin intercity railway, Shanghai-Hangzhou HSR, and several other HSRs in China whose design speed is 350 km/h. It consists of continuously welded rails, fasteners, prefabricated slabs connected longitudinally by concrete joints, a layer of mortar, and a concrete base, as shown in Fig. 1. Interfacial gaps, slab end arching, slab and concrete base cracks, joint concrete crushing, and mortar crushing have been observed for several track segments (Zhou et al., 2023a; Xu et al., 2021; Wang et al., 2019; Ye et al., 2022; Cui et al., 2021). Among those types of damages, interfacial gaps between the concrete slabs and the mortar layer, and slab end arching are the most critical (as shown in Fig. 2), since the original track layers are delaminated and therefore harmfully affect the integrity of the track structure, impairing dynamic interactions between the tracks and highspeed trains (Xu et al., 2022).

Analytical, numerical, and experimental studies have been conducted to determine the effects of train axle load, temperature, and hydrodynamic pressure on the initiation and development of the damages (Zhu and Cai, 2014; Zhou et al., 2023b; Cao et al., 2016). It is reported that the difference in deformation between the concrete slabs and the mortar layer induced by temperature changes is the main factor that causes interface damage (Liu and Zhao, 2013). A cohesive zone model

* Corresponding author.
E-mail addresses: sakdirat@hotmail.com, s.kaewunruen@bham.ac.uk (S. Kaewunruen).

https://doi.org/10.1016/j.dibe.2023.100204
Received 14 May 2023; Received in revised form 23 July 2023; Accepted 24 July 2023
Available online 27 July 2023
2666-1659/© 2023 The Authors. Published by Elsevier Ltd. This is an open access article under the CC BY license (http://creativecommons.org/licenses/by/4.0/).

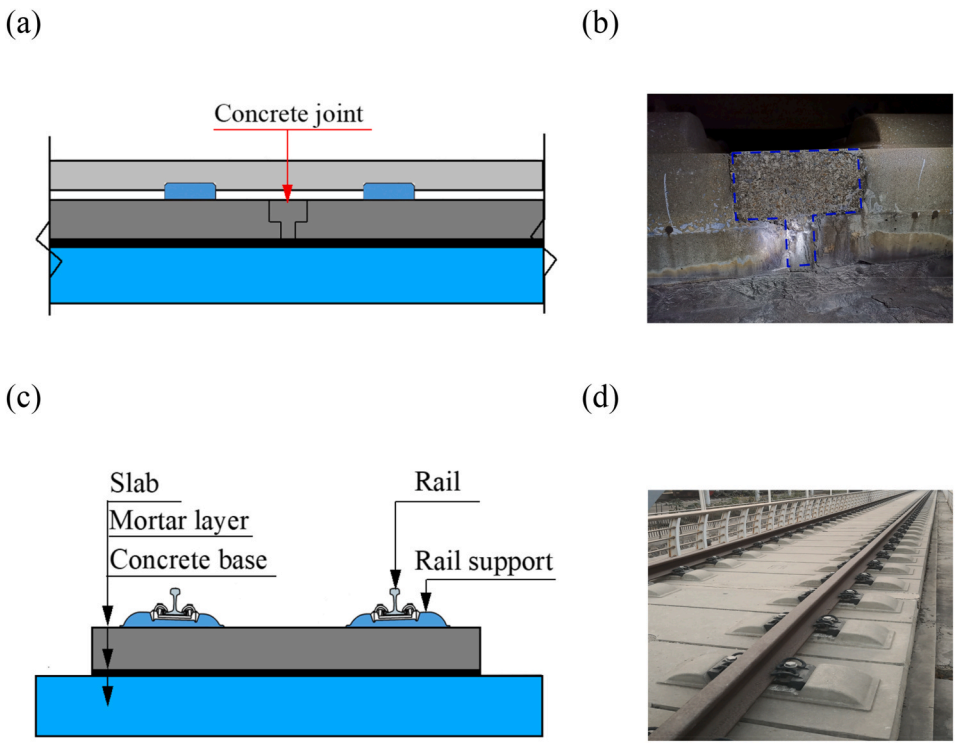

Fig. 1. Illustration of the structure of the longitudinally continuous slab track with (a) side view of the track structure, (b) photo of the concrete joint (c) front view of the track structure, and (d) photo of actual track structure.

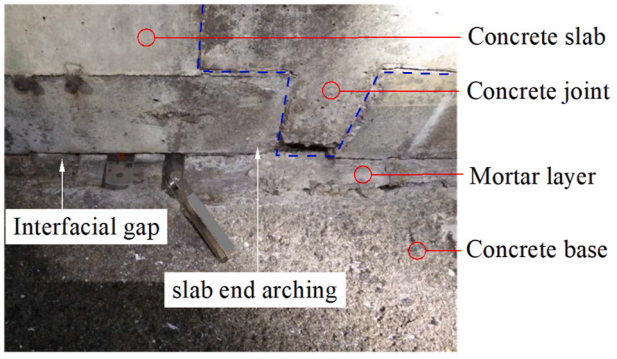

Fig. 2. Actual photo of the longitudinally continuous slab track with damages like the interfacial gap between concrete slabs and mortar layers, and slab end arching.

has been proven to be capable of simulating the interfacial cracking and debonding behavior of laminated composite structures (Chen et al., 2019a, 2019b, 2021). And it has been widely used to study the damage of the interfaces between track slabs and mortar layers of railway slab tracks (Xu et al., 2022; Zhu and Cai, 2014). In summer, the track structure is subjected to both high levels of temperature rise and temperature gradient, which may cause severe interface damage and slab end arching (Matias and Ferreira, 2022). In addition, the mechanical properties, which are greatly related to construction quality, are also crucial for the structural integrity of the interface (Matias and Ferreira, 2022). During construction, air bubbles can gather on the upper surface of the mortar layer other than the lower surface due to the effect of gravity, resulting in lower bond strength at the interface between the slabs and the mortar layer than that between the mortar layer and the concrete base (Liu et al., 2011). Fatigue behavior and damage of slab tracks have also been investigated (Heng et al., 2020). Khajehdezfuly et al. (2023) studied the influences of track flexibility on the fatigue life of slab tracks. Yang et al. (2022) analyzed the evolution of fatigue damage of track slabs and predicted their fatigue life. Tarifa et al. (2015) conducted full-scale experimental tests to investigate the fatigue behavior of precast reinforced track slabs. Deng et al. (2021) researched the fatigue damage of the mortar layer of ballastless tracks based on the finite element method.

Several repair methods have been adopted in the railway industry to cope with the interface damages found in the longitudinally continuous slab tracks. Cracked interfaces are generally repaired by adhesive materials like low-viscosity grouting resin (Yi et al., 2015). Crushed joints and broken slabs should be replaced (Mao, 2020). Post-installed anchors can be used to connect several adjacent track slabs and the concrete base before replacing the damaged joint or track slab, in order to prevent the differential displacement of adjacent track slabs (Ni et al., 2016; Li et al., 2021a). Since 2017, in several HSRs in East China, anchors have been installed in all the track slabs and the concrete base to enhance the integrity of the track structures and prevent any possible damage (Zhao et al., 2021).

Post-installed anchors have been proven to be effective as the number of damages has reportedly declined after the installation of anchors (Zhao et al., 2021). Finite element simulation results also indicated that post-installed anchors could reduce the differential deformation and displacement of the tracks (Li et al., 2021a). However, even though tracks have been reinforced by anchors, damages including interfacial gaps can still occur due to high temperatures in summer (Li et al., 2022a). Thus, some other measures, like solar reflective coatings, may be taken to further improve the damage resistance of the longitudinally continuous slab tracks over the long run.

In addition to post-installed anchors, solar reflective coatings are also seen as a promising solution to mitigate the damages of slab tracks caused by elevated temperatures. While post-installed anchors intend to reinforce the tracks, solar reflective coatings resolve the issue by reducing heat absorption and therefore lowering the temperature absorbed by the track (Li et al., 2022b). Several solar reflective coatings, such as metal-ceramic anticorrosion coating and fluorocarbon coating,

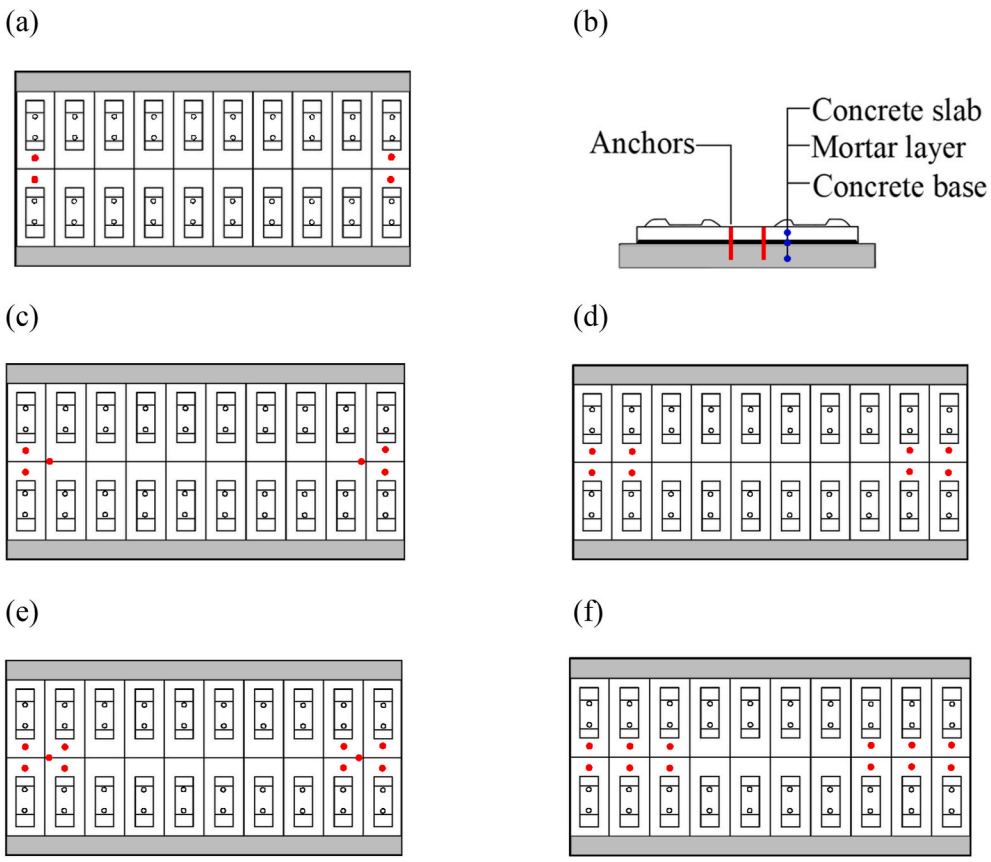

Fig. 3. Scenarios of quantities of anchors in a track slab with (a) top view of the track slab with 4 anchors, (b) front view of the track slab with 4 anchors, (c) top view of the track slab with 6 anchors, (d) top view of the track slab with 8 anchors, (e) top view of the track slab with 10 anchors and (f) top view of the track slab with 12 anchors.

have been developed for the railway industry (Kang, 2018; Li et al., 2021b; Zhang et al., 2020). However, its consequence towards structural damages has not been thoroughly assessed.

To cope with the temperature-induced problems in the railway tracks, solar reflective coatings are likely to be used on both traditional tracks and anchor-reinforced tracks. Therefore, it is of great practical value and necessity to identify the performance of anchor-reinforced and coated longitudinally continuous slab tracks. However, to our knowledge, there is no previous research that has studied the coupling effects of the dual applications of anchors and coatings on the damages of the longitudinally continuous slab tracks. In addition, the efficiency of different track maintenance methods in mitigating HSR track damages has not been comparatively investigated. The lack of such insights will impede progresses for rail decarbonisation towards net zero (Kaewunruen et al., 2023; Sresakoolchai and Kaewunruen, 2023).

In this paper, temperature-induced damages such as interface debonding and slab end arching of anchor-reinforced and coated longitudinally continuous slab tracks have been investigated. A novel finite element model of the longitudinally continuous slab track has been established, and the cohesive zone model to represent the nonlinear constitution relationships has been incorporated into the nonlinear finite element model. This study highlights the effects of dual applications of post-installed anchors and solar reflective coatings on the development of interface damage and slab end arching. In particular, the efficiency of different HSR track maintenance measures has been compared, which is of great necessity for track maintenance method selection. It is noted that the influence of different quantities of anchors and varied types of coatings on the performance of the longitudinally continuous slab tracks has been explored in detail. The insight of this study will help track engineers optimize track maintenance strategies, thereby improving the reliability and sustainability of rail infrastructure systems.

2. Applications of anchors and coatings

Anchors are installed symmetrically at both ends of a track slab to prevent slab end arching due to elevated temperature. Four anchors in a track slab are the most common case. Six, eight, ten, and twelve anchors in a track slab can also be used, as shown in Fig. 3. The diameter and length of the anchor are 27 mm and 350 mm respectively, which are the same as the values used in practice. Embedment depths in the track slab, the mortar layer, and the concrete base are 160 mm, 30 mm, and 160 mm respectively. In practice, anchors can be placed into the boreholes after adhesives are injected into the boreholes. In this way, the anchors can be bonded with the surrounding concrete in the boreholes. The waterproof material is used to cover the top of the anchors.

Bond-slip relationships between the anchors and the concrete provide essential mechanical parameters for the finite element model. Pull-out tests have been carried out by Li et al. (2022a) to determine the bond-slip relationships between the anchors and the concrete. A detailed illustration of the anchor pull-out test can be found in Reference (Li et al., 2022a). Based on the pull-out tests, for anchors and the concrete with standard cube compressive strength of C55 used for track slabs, the bond strength and corresponding slip are 12.975 MPa and 1.091 mm respectively, and the bond-slip relationships are as follows:

$$\tau = \begin{cases} 30.15S, 0 \le S < 0.26 \\ 6.181(S - 0.26) + 7.839, 0.26 \le S < 1.091 \end{cases} \quad (1)$$

In which τ is the mean bond stress between the anchors and the concrete, whose unit is MPa, and S is the mean relative slip between the

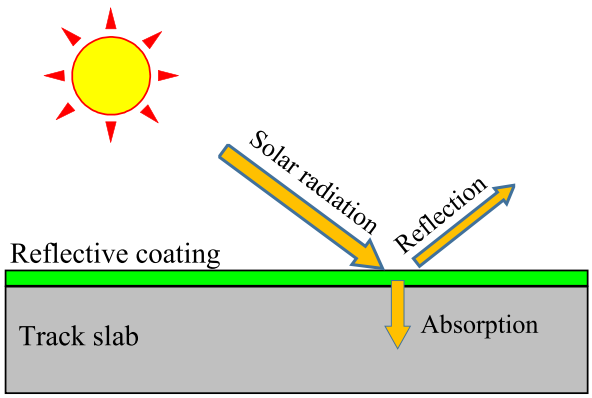

Fig. 4. Illustration of the effect of solar reflective coatings which are capable of reflecting more solar radiation.

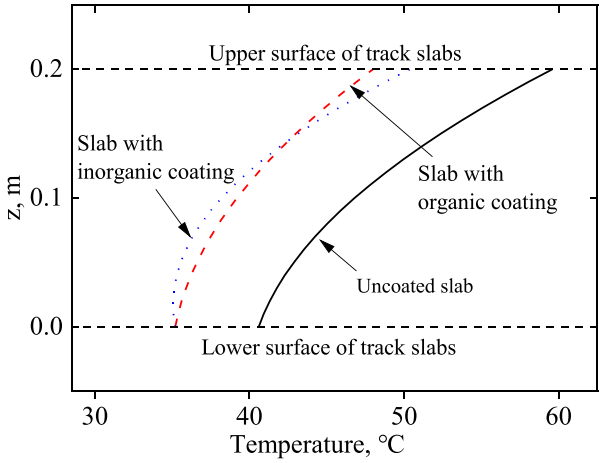

Fig. 5. The maximum vertical temperature distribution in the track slabs whose thickness is 0.2 m, z is the height to the slab bottom.

anchors and the concrete, whose unit is mm.

For anchors and the concrete with standard cube compressive strength of C30 used for the concrete base, the bond strength and corresponding slip are 11.992 MPa and 2.042 mm respectively, and the bond-slip relationships are as follows:

$$\tau = \begin{cases} 20.043S, 0 \le S < 0.317 \\ -1.897S^2 + 7.748S + 4.082, 0.317 \le S < 2.042 \\ -0.574S + 13.164, 2.042 \le S < 4.446 \end{cases} \quad (2)$$

Solar reflective coatings are designed to lower the temperature of the track structures, especially the mass concrete slabs, by reflecting solar radiation in summer, as shown in Fig. 4. Several types of solar reflective coatings have been developed, among which an organic coating and an inorganic coating developed by Kang et al. (Kang, 2018) have been tested on a full-scale longitudinally continuous track prototype located in Shanghai, which is very close to the actual situation of application. The temperature change of the track slabs for the uncoated track slabs, the slabs coated by the organic coating and the inorganic coating during the summer was recorded. It has been found that the vertical temperature distribution in track slabs is nonlinear. Choubane et al. (Choubane and Tia, 1992) found that the maximum vertical temperature distribution in a concrete slab can be defined by a quadratic function. Therefore, based on the measurement data by Kang et al. (Kang, 2018) and the quadratic function by Choubane et al. (Choubane and Tia, 1992), the maximum vertical temperature distribution of track slabs can be obtained.

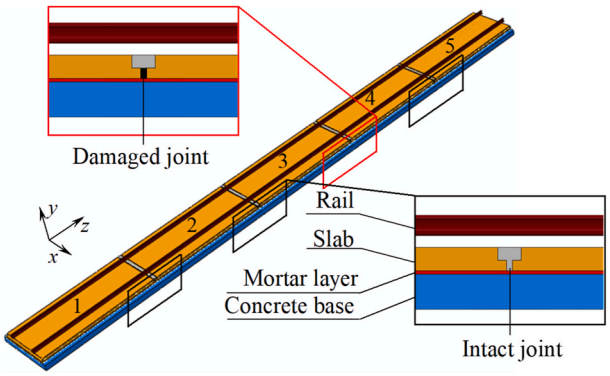

Fig. 6. Finite element model of the longitudinally continuous slab track with 5 track slabs labeled with numbers 1 to 5.

For the uncoated track slabs, the maximum vertical temperature distribution is determined as follows:

$$T(z) = 40.6 + 29z + 330z^2 \quad (3)$$

In which, $T(z)$ is the temperature at the location of z, and z is the height to the slab bottom, whose unit is m.

For the organic coating, the equation is

$$T(z) = 35.2 + 16z + 240z^2 \quad (4)$$

For the inorganic coatings, the equation is

$$T(z) = 35.2 - 16z + 460z^2 \quad (5)$$

Temperature distribution in the track slabs with different coatings are shown in Fig. 5.

The temperature gradients in the mortar layer and concrete base are so small that they can be negligible (Zhao and Liu, 2020). Therefore, the temperature of the mortar layer and concrete base can be considered to be equal to the temperature of the slab bottom (Li et al., 2022a).

3. Finite element model

3.1. Finite element modelling of the track structure

A nonlinear finite element model of the longitudinally continuous slab track structure has been established by ABAQUS, as shown in Fig. 6. It consists of 2 rails, 100 fasteners, 5 track slabs connected by 4 concrete joints, a layer of mortar, and a concrete base. The length, width, and thickness of a track slab are 6.45 m, 2.55 m, and 0.2 m respectively. The width and thickness of the mortar layer are 2.55 m and 0.03 m respectively. The width and thickness of the concrete base are 2.95 m and 0.3 m respectively. The track slabs are installed on railway viaducts, which are widely adopted in China since they take up less agricultural land, and 32 m simply-supported girders are one of the most popular bridge supports. The total length of the track model equals the length of a 32 m simply-supported girder. For the coordinate system, the axis of x is in the lateral direction of the track, y is in the vertical direction, and z is in the longitudinal direction.

Due to poor construction quality, damage of the narrow part of the joint is commonly found in the longitudinally continuous slab tracks, which can result in slab end arching and interface damage (Gao et al., 2020). Therefore, the joint between track slabs labeled 3 and 4 is considered as a damaged joint, in which the elements of the narrow part are deleted, and other joints are considered as intact, as shown in Fig. 6.

Solid element type C3D8R is used for the rails, the track slabs, the concrete joints, the mortar layer, and the concrete base. Beam element type B33 is used to simulate the anchors, and nonlinear spring elements have been utilized to represent the interaction between the anchors and the surrounding concrete in the vertical direction (y), as described in Eq

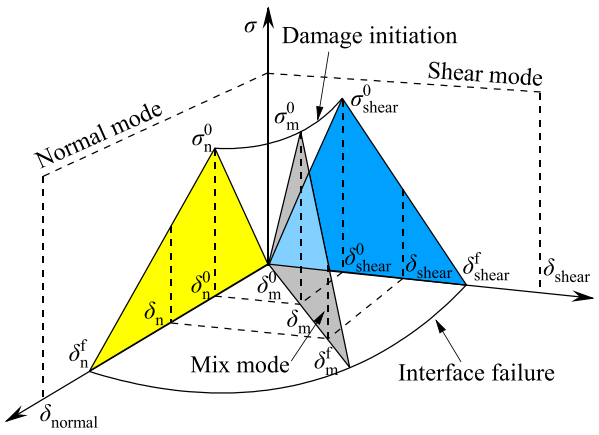

Fig. 7. Bi-linear cohesive law in the mixed mode with bi-linear bond stress-displacement relationship in both normal direction and shearing directions.

(1) and Eq (2). In the longitudinal (z) and the lateral (x) directions, there is very minor displacement between the anchors and the surrounding concrete, so spring elements with a large stiffness of 1×10^8 N/mm have been used to simulate the interaction in the longitudinal and the lateral directions. Fasteners are simulated by spring elements with bilinear force-displacement interaction, as defined in Reference (Li et al., 2022a). Standard cube compressive strength for the concrete of track slabs, joints, and concrete base are C55, C55, and C30 respectively. The concrete damaged plasticity model is applied to represent the nonlinear constitutive properties of the concrete. Detailed descriptions and material parameters for the model can be found in References (Lubliner et al., 1989; Ren et al., 2019; Ministry of Housing and Urban-Rural Development of the People's Republic of China, 2014). Material properties for other track components are considered linear, since their strains should be within the elastic range under the thermal load considered in this paper, and their material parameters can be found in Reference (Li et al., 2022a).

The damage usually initiates and propagates on the interface between the track slabs and the mortar layer, so a cohesive zone model described in Section 3.2, which can mimic interface damage evolution, is used for this interface. Other interfaces between track components are not prone to any damage under temperature rise, so they are tied. The lower surface and the two ends of the track structure are fixed to simulate the constraint of the girder and the neighboring track segments on the slab track. The temperature loading is simulated by changing the predefined temperature field of the track. The maximum temperatures of the track structures under different coating strategies defined in Section 2 are used in the simulations. The temperature of the zero-stress state for the track is considered to be 15 °C. Accordingly, the temperature rise in the finite element analysis will be equal to the maximum temperatures subtracted by 15 °C (Li et al., 2022a). The gravity of the track is considered and the acceleration of gravity is taken as 9.8 m/s^2. General static analysis has been conducted in the simulation.

The finite element model established in this paper enables the simulation of the combined use of anchors and coatings in slab tracks and promotes the understanding of the mechanical behavior of the reinforced and coated tracks subjected to temperature change.

3.2. Cohesive zone model for the interface

Previous studies show that the interface between the track slabs and the mortar layer presents a nonlinear bond stress-displacement relationship in both normal direction and shearing directions (Zhu and Cai, 2014). The bilinear cohesive zone model, capable of simulating brittle fracture behaviors under the mixed mode of normal and shearing displacements depicted in Fig. 7, is considered to be suitable to represent

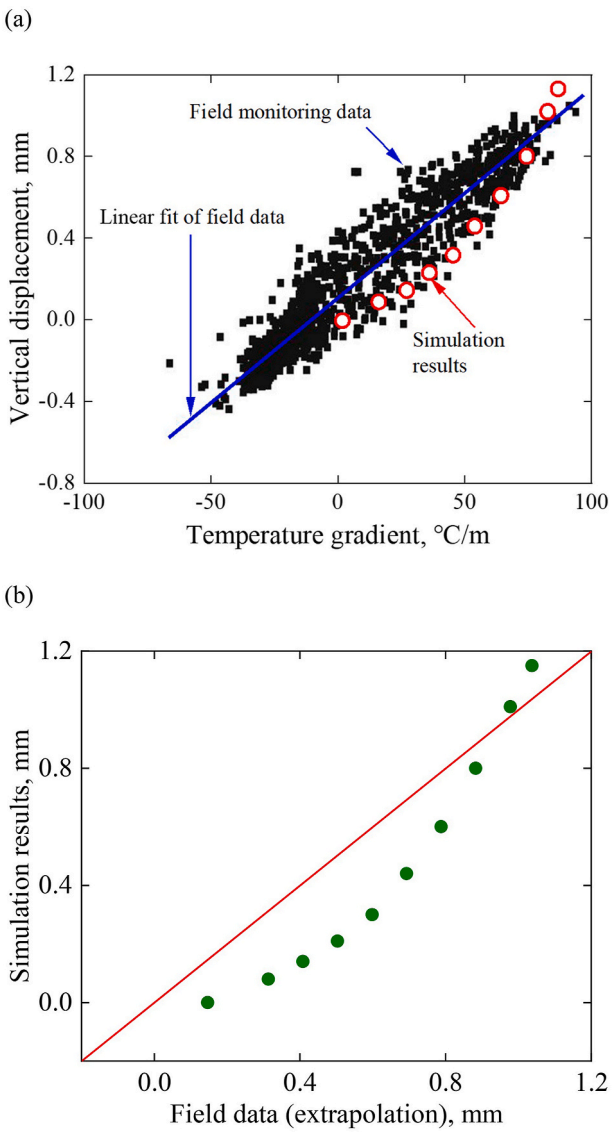

Fig. 8. (a) comparison between monitoring and simulation data with vertical displacement versus temperature gradient, (b) correlation between monitoring and simulation data.

both the bond stress-displacement relationship and the damage evolution of the interface.

In the simulation, 8-node cohesive elements whose thickness is zero have been embedded between the track slabs and the mortar layer. Damage of the cohesive elements is initiated when

$$\left\{\frac{\langle\sigma_n\rangle}{\sigma_n^0}\right\}^2+\left\{\frac{\sigma_s}{\sigma_s^0}\right\}^2+\left\{\frac{\sigma_t}{\sigma_t^0}\right\}^2=1 \tag{6}$$

Where σ represents the bond stress. The subscripts n, s, and t mean the normal direction, the first shearing direction, and the second shearing direction respectively. $\langle\sigma_n\rangle=(\sigma_n+|\sigma_n|)/2$.

After the damage is initiated, the interface undergoes a softening process and the bond stress-displacement relationships can be described as:

$$\begin{aligned}\sigma_n&=\begin{cases}(1-D)k_n\delta_n, \delta_n>0\\ k_n\delta_n, \delta_n\le 0\end{cases},\\ \sigma_s&=(1-D)k_s\delta_s,\\ \sigma_t&=(1-D)k_t\delta_t\end{aligned} \tag{7}$$

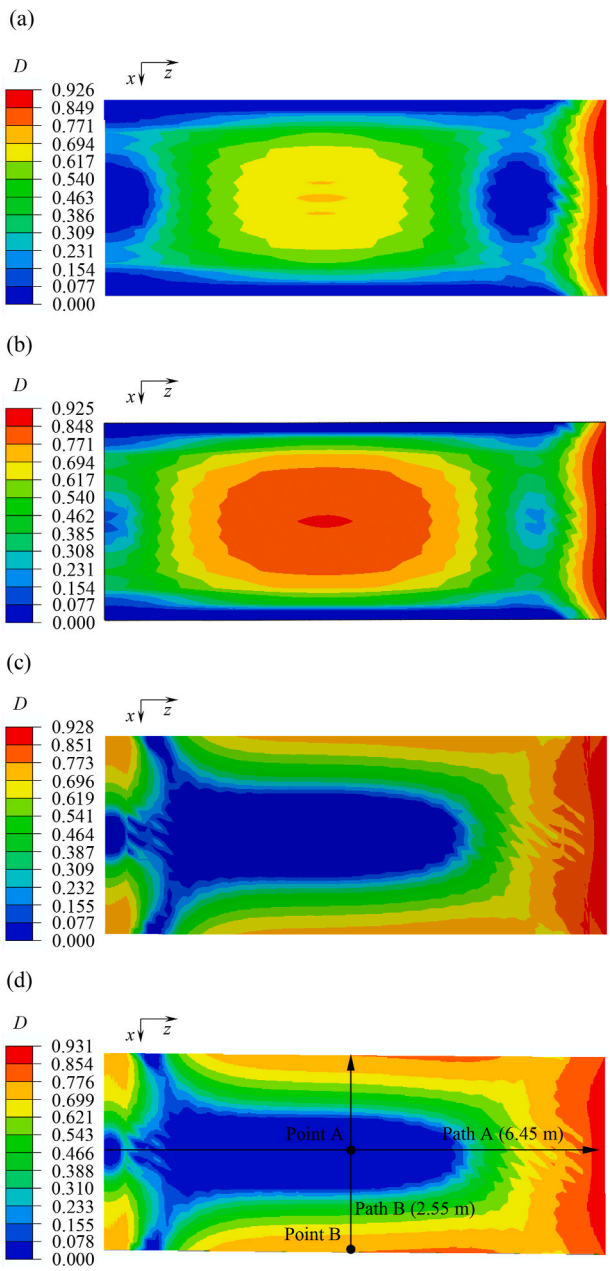

Fig. 9. Contours of interface damage for the track with (a) 4 anchors in each slab and organic coating, (b) 4 anchors in each slab and the inorganic coating, (c) 6 anchors in each slab and the organic coating and (d) 6 anchors in each slab and the inorganic coating.

Where k refers to the penalty stiffness, and D is a damage variable expressed as:

$$D = \frac{\delta_m^f\left(\delta_m^{max} - \delta_m^0\right)}{\delta_m^{max}\left(\delta_m^f - \delta_m^0\right)} \tag{8}$$

Where δ_m^{max} donates the maximum effective displacement during the loading history, δ_m^0 and δ_m^f refer to the effective displacements at damage initiation and failure of the interface respectively.

D with the value of 0 shows that no damage has occurred for the cohesive element, and D with the value of 1 represents a complete failure of the cohesive element. D between 0 and 1 indicates that the damage has evolved.

The interface is considered to fail when the following equation satisfies

$$\left\{\frac{G_n}{G_n^C}\right\}^2 + \left\{\frac{G_s}{G_s^C}\right\}^2 + \left\{\frac{G_t}{G_t^C}\right\}^2 = 1 \tag{9}$$

Where G means the work done by the bond stress and the displacement, and G_C represents critical energy release rate corresponding to the interface failure.

The parameters of the cohesive zone model are determined in Ref (Li et al., 2021a). Since the temperature doesn't go beyond the normal temperature range in this paper, the effects of temperature on the parameters of the cohesive zone model have been neglected.

3.3. Model verification

Field monitoring for the longitudinally continuous slab track on the simply-supported beam bridges was conducted by Tan et al. (2020). The temperature at the top and the bottom of the track slab was measured by temperature sensors so that the temperature gradient of the track slab could be calculated. The relative vertical displacement between the track slab and the concrete base was measured by LVDTs located at the end of the track slab. The field-collected data in Fig. 8(a) suggests that the relative vertical displacement between the track slab and the concrete base shows an increased trend with a rising temperature gradient (Tan et al., 2020). A finite element model of the track using the modeling techniques described above has been established accordingly. The simulation results are also shown in Fig. 8(a). It can be found that the simulation results are within the scope of field monitoring data. The

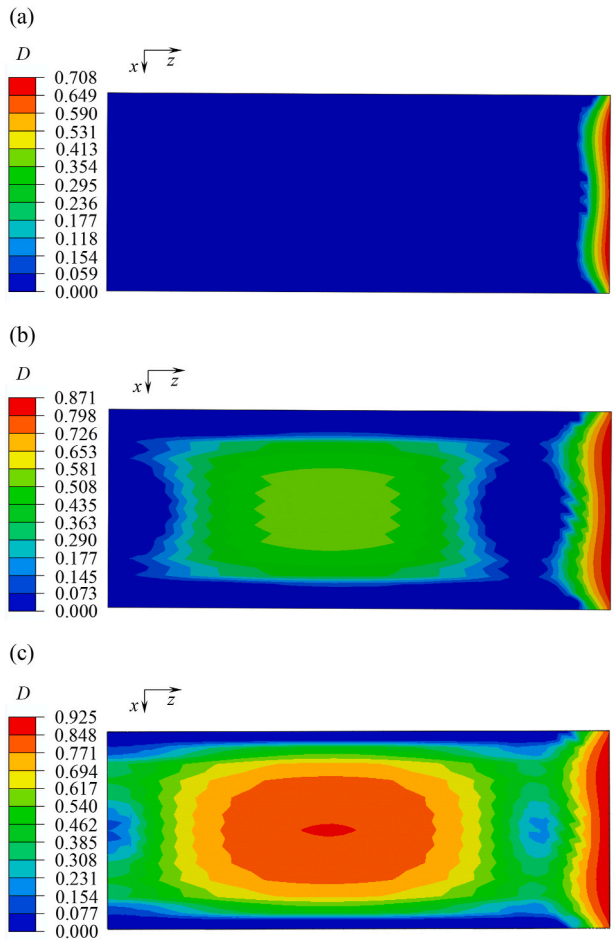

Fig. 10. Contours of interface damage of the track slab with 4 anchors and inorganic coating (a) with a temperature rise of 16.8 °C, (b) 27.4 °C and (c) 35.4 °C respectively.

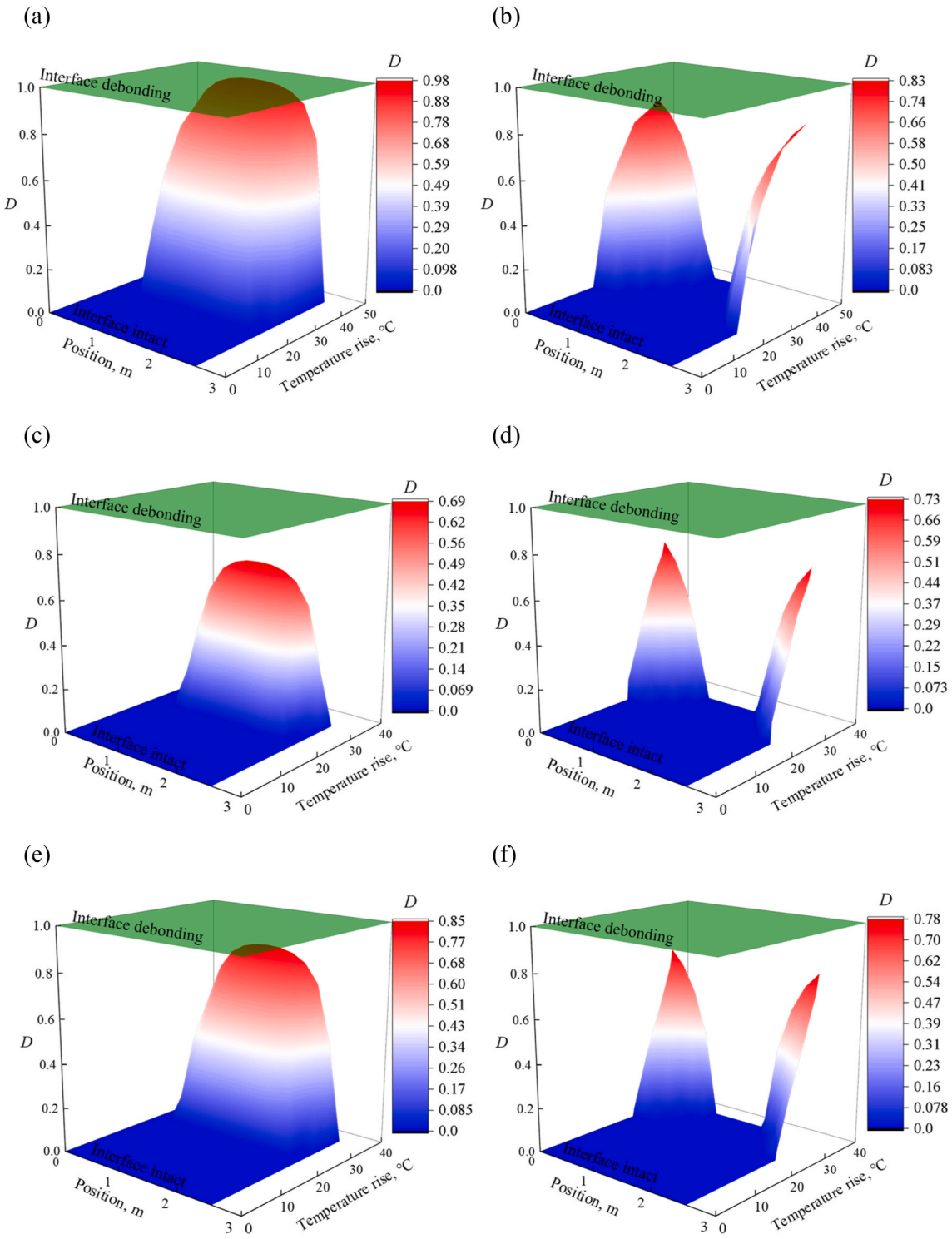

Fig. 11. Development of interface damage in path B for (a) the uncoated track with 4 anchors in each slab, (b) the uncoated track with 6 anchors in each slab, (c) the track coated by the organic coating with 4 anchors in each slab, (d) the track coated by the organic coating with 6 anchors in each slab, (e) the track coated by the inorganic coating with 4 anchors in each slab and (f) the track coated by the inorganic coating with 6 anchors in each slab.

correlation between the field monitoring data and the simulation data is presented in Fig. 8(b). It can be known from Fig. 8(b) that the simulation results are close to the monitoring data. Therefore, the above-mentioned techniques are capable of simulating the mechanical performance of the longitudinally continuous track.

4. Results and discussion

Vehicle passages and temperature changes have been considered as two main sources of external loading for railway slab tracks. While train loads applied to the slab track can cause deterioration of track components during the life of slab tracks, significant temperature rises in the short-term can induce structural damage of the slab tracks. In this paper, the influences of elevated temperature in the short-term have been

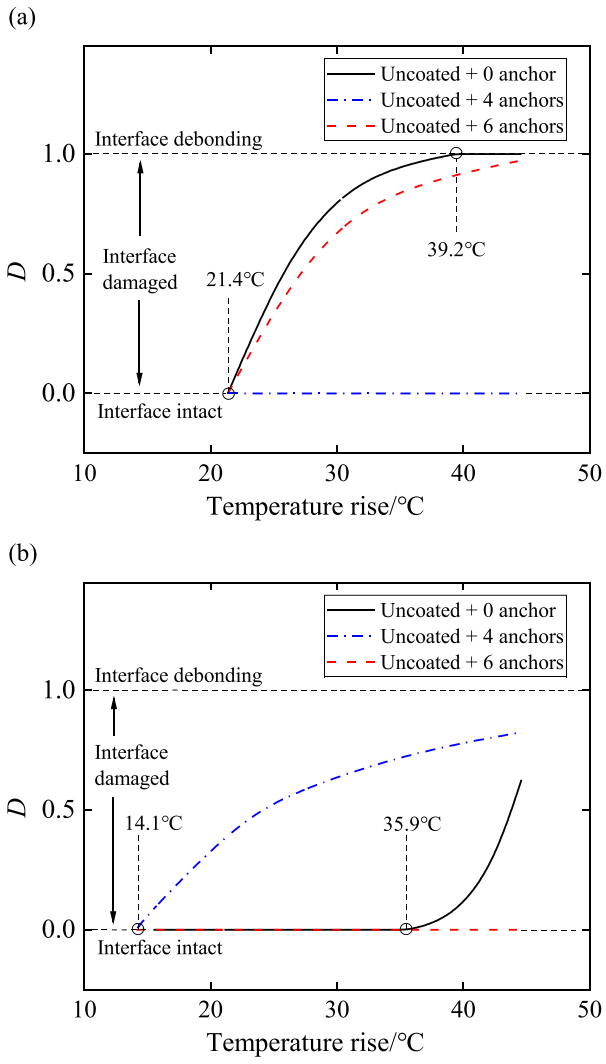

Fig. 12. Development of interface damage for the uncoated longitudinally continuous slab track with temperature rise at (a) point A and (b) point B.

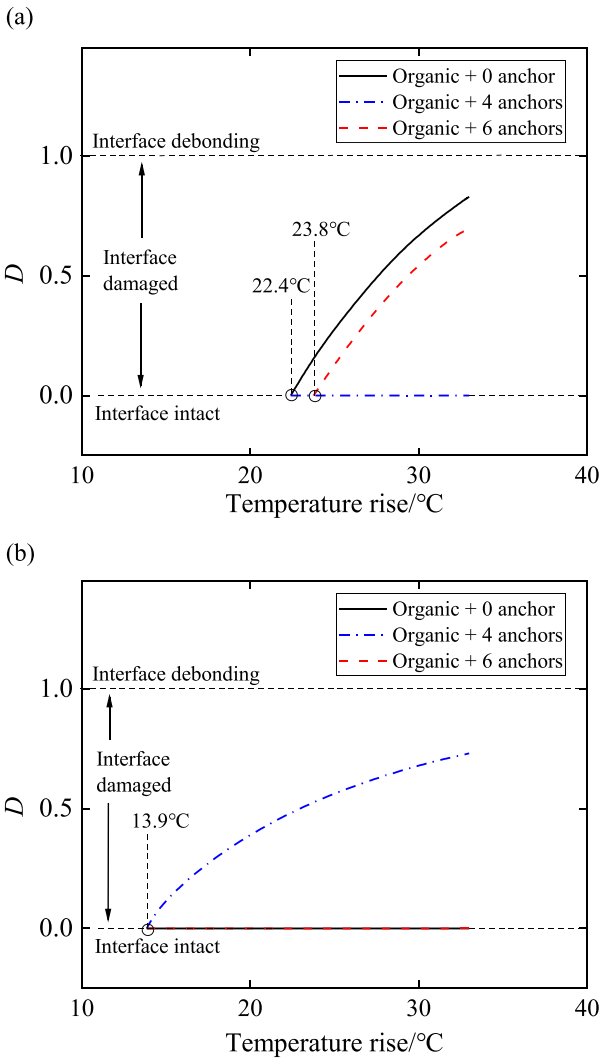

Fig. 13. Development of interface damage for the longitudinally continuous slab track with the organic coating with temperature rise at (a) point A and (b) point B.

evaluated while the effects of repeated train loads have been neglected.

4.1. *Effect of repair methods on the interface damage*

Fig. 9 presents the contours of the interface damage variable *D* with different combinations of anchor quantities and coating types. Note here that the interface is between the mortar layer and the track slab labeled with 3 in Fig. 6, and the right end of the track slab is adjacent to the damaged joint. It can be known that for the same anchor quantities but different coating types, the interface damage distribution follows the same pattern, while for the same coatings but different anchor quantities, the interface damage distribution can be significantly different. To better show the detailed differences of interface damage, two paths and two points on the interface between the mortar layer and the track slab labeled with 3 in Fig. 6 are defined in Fig. 9(d). *D* in different paths and points will be compared in the following text.

High temperature has been considered as the main cause of interface damage of longitudinally continuous slab tracks (Yan et al., 2016; Kang et al., 2019; Zhou et al., 2022, 2023c; Zhang et al., 2022). Fig. 10 shows the contours of *D* for the interface with 4 anchors and the inorganic coating with different temperature rises. It can be found that the interface damage initiates from the right end of the interface, which is close to the damaged joint. With a temperature rise of 27.4 °C, the middle of the interface is also damaged, but the area near the anchors remains intact. When the temperature rise reaches its maximum of 35.4 °C, most of the interface is damaged, while damage for the interface area near the anchors is milder than other area. It indicates that anchors can reduce local interface damage and therefore improve the long-term serviceability of the longitudinal track (Dai and Su, 2016; Lou et al., 2015; Li et al., 2020; Qi et al., 2015; Dai and Li, 2016; Xiao et al., 2018; Zhong et al., 2018; Mahaboonpachai et al., 2010).

Fig. 11 demonstrates the development of the interface damage in path B. It can be known that the interface damage initiates in the middle of path B for the track with 4 anchors in each track slab, and emerges at two ends of path B for the track with 6 anchors in each track slab. Note here that "temperature rise" in Fig. 11 refers to the temperature rise of the slab's upper surface. Since temperature is not linearly distributed across the track profile (as shown in Fig. 5), the temperature rise below the slab's upper surface can be slightly different from the temperature rise of the slab's upper surface. It can be found from Fig. 11 that the temperature rise to interface damage initiation for the uncoated track is smaller than that for the coated tracks when the anchor quantities of those tracks are the same. However, the damage will initiate in path B with a temperature rise over 25 °C, no matter coatings are used or not.

The development of interface damage for the uncoated track at points A and B is depicted in Fig. 12. It can be found from Fig. 12(a) that interface damage will initiate at 21.4 °C, and that interface debonding

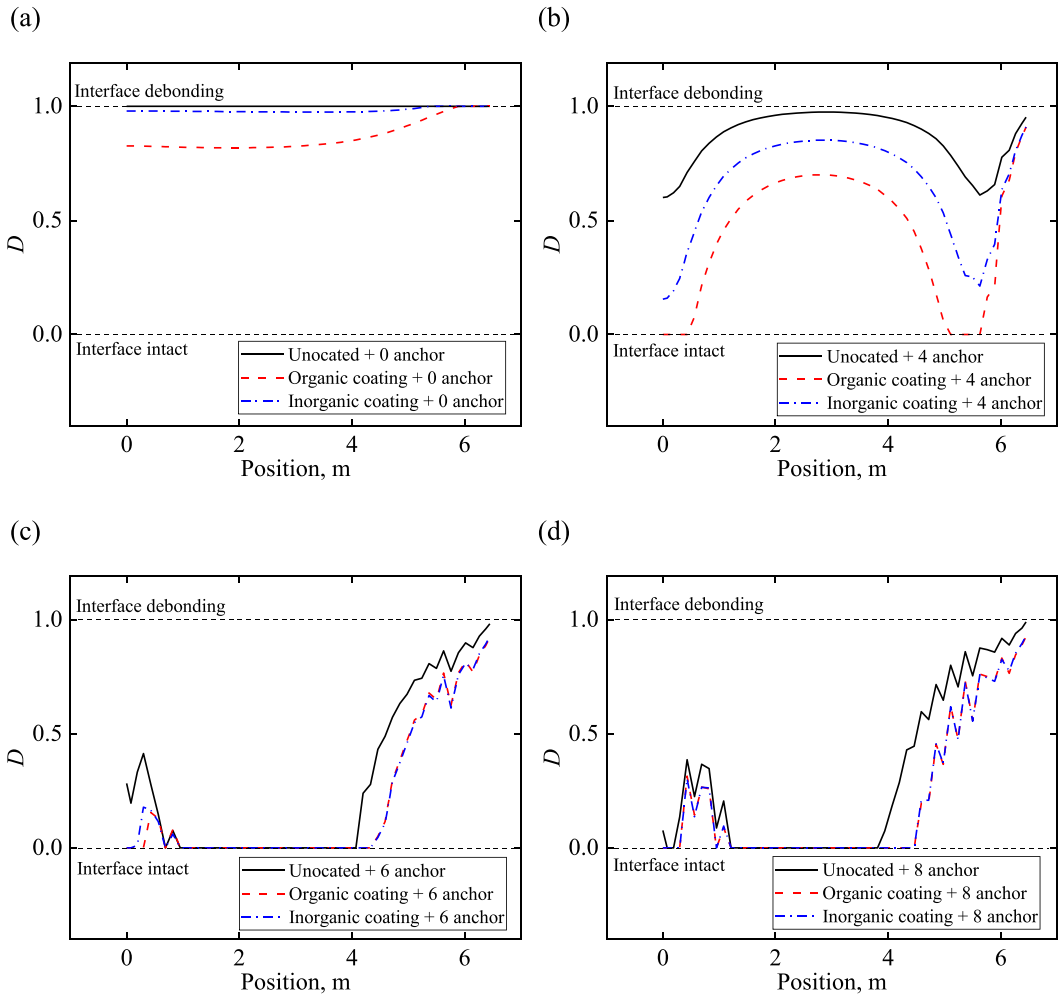

Fig. 14. Interface damage in path A for the longitudinally continuous slab track with (a) 0 anchors, (b) 4 anchors, (c) 6 anchors, and (d) 8 anchors.

will occur at 39.2 °C at point A for the uncoated track with no anchors. When 6 anchors are used in each slab for the uncoated track, the interface at point A will be damaged at 21.4 °C, but no interface debonding will emerge even the temperature reaches its highest. When 4 anchors are used in each slab for the uncoated track, no interface damage at point A will occur. It can be known from Fig. 12(b) that interface damage will initiate at 35.9 °C at point B for the uncoated and unreinforced track. For the uncoated slabs with 4 anchors, interface damage will initiate at point B at 14.1 °C which is a very low temperature, meaning that the position is prone to interfacial damage in this scenario.

Fig. 13 depicts the development of interface damage for the track coated with the organic coating at points A and B. It can be found from Fig. 13(a) that interface damage will initiate at 22.4 °C at point A for the coated track with no anchors, but no interface debonding will emerge even the temperature reaches its highest. When 6 anchors are used in each, the interface at point A will be damaged at 23.8 °C. When 4 anchors are used in each slab, no interface damage at point A will occur. It can be known from Fig. 13(b) that interface damage will initiate at 13.9 °C at point B for the coated track with 4 anchors in each slab.

Fig. 14 depicts D in path A for the track with different combinations of anchor quantities and coating types. Fig. 14(a) shows that for the track without anchor reinforcement, the interfaces along path A for the uncoated track and the track with inorganic coating almost completely fails under temperature rise, as their D equals or is very close to 0, while the interface along path A for the track with the organic coating is damaged but not completely debonded as most of its D is between 0 and 1. Fig. 14(b) suggests that D at or near the locations of anchors is smaller than others, indicating the effects of anchors on mitigating the interface damage, and that the organic coating significantly outweighs the inorganic coating to improve interface damage mitigation. In comparison with the track with 4 anchors in each track slab in Fig. 14(b) and (c) shows a totally different interface damage pattern for the track with 6 anchors in each track slab: The interface is intact in the middle of path A, and the interface damage near the damaged joint is much severer than that near the intact joint. In addition, D for the track with the organic coating is slightly smaller than D for the track with the inorganic coating. As shown in Fig. 14(d), the interface damage in path A for the track with 8 anchors in each track slab follows the same pattern as the track with 6 anchors in each track slab.

Fig. 15 shows D in path B for the track with different combinations of anchor quantities and coating types. It can be seen that D in path B follows one pattern for 0 and 4 anchors in each track slab, and another pattern for 6, 8 anchors in each track slab (10 and 12 anchors in each track slab follow the latter pattern and thus are not depicted). In the former case, D in the middle of path B is larger than that at its two ends. In the latter case, the middle of path B is intact, while the two ends of path B are damaged. The interfacial damage or debonding in the middle of path B can be harmful to the stability of the longitudinally continuous slab tracks and thus should be avoided (Wang and Xia, 2012; Xu et al., 2013; Yang et al., 2016; Liang et al., 2023; Zhao, 2017). For all the scenarios, D for the coated track is smaller than D for the uncoated tracks, and the organic coating performs better than the inorganic coating in terms of mitigating interface damage in path B.

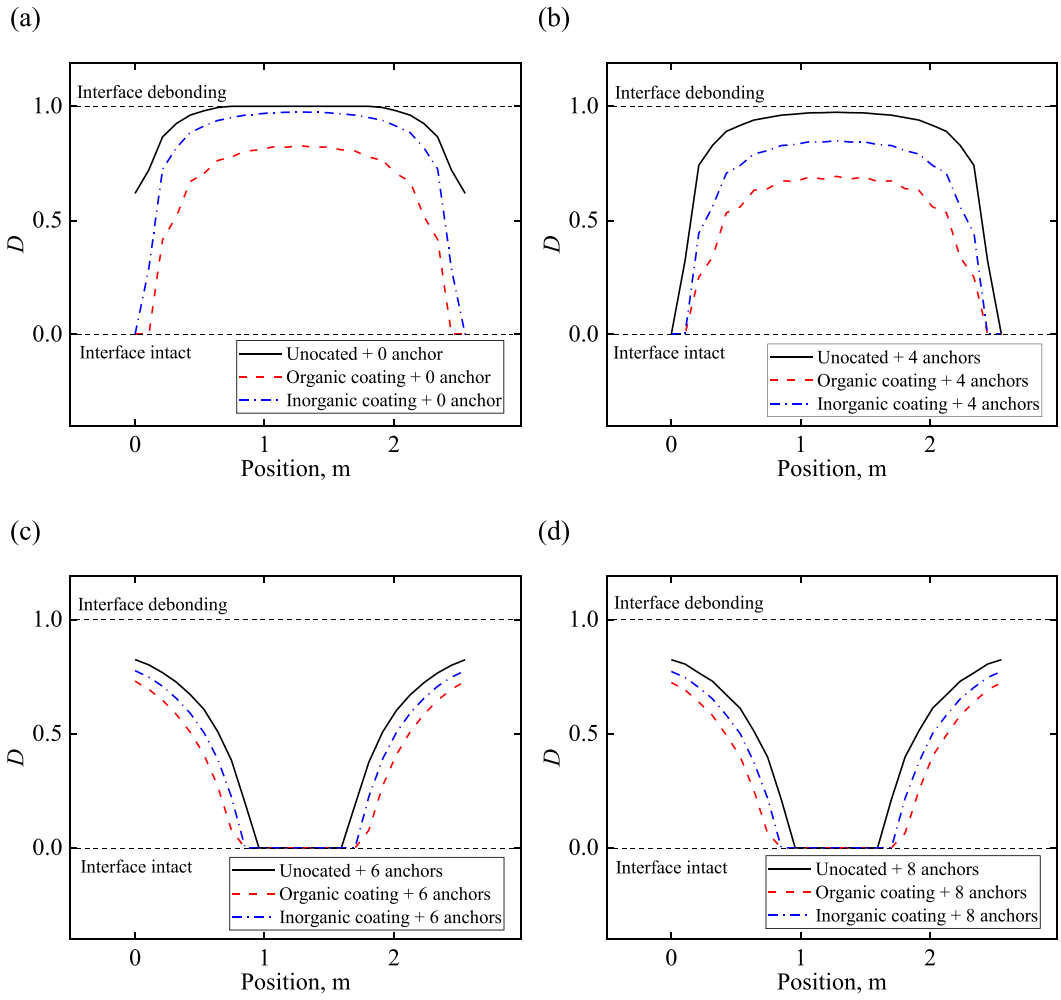

Fig. 15. Interface damage in path B for the longitudinally continuous slab track with (a) 0 anchors, (b) 4 anchors, (c) 6 anchors, and (d) 8 anchors.

Interface damage can be caused by the interlayer separation, interlayer slide, or both of them. To better analyze the mechanism of the interface damage for the track, Fig. 16 shows the vertical relative displacement (U_y) and longitudinal relative displacement (U_z) between the track slab labeled with 3 in Fig. 5 and the mortar layer in path A for the track with different combinations of anchors and coatings. Note here that the lateral relative displacement is zero in path A thus not provided. It can be found from Fig. 16(a) that for the track with 0 anchor in each track slab, U_y is larger than U_z, and the relative displacements for the coated track are smaller than those of the uncoated track. Besides, the organic coating is more capable of decreasing the relative displacements than the inorganic coating. It can be known from Fig. 16(b) and (c) that for the track with 4 and 6 anchors in each track slab, the above-mentioned rules are also followed. However, in comparison with Fig. 16(a), U_y in Fig. 16(b) and (c) presents different maximum values and shapes. On the one hand, compared with the condition of 0 anchor in a track slab, the maximum value of U_y drops significantly when there are anchors. On the other hand, it can be found from Fig. 16(a) that U_y near end A is much larger than other positions for 0 anchor in each track slab, from Fig. 16(b) that U_y in the middle of path A U_y can be larger than its two ends for the track slabs with 4 anchors. Moreover, Fig. 16(c) suggests that U_y in the middle of path A is generally eliminated for the track slabs with 6 anchors, as more anchors prevent the arching in the middle of the slabs. For the track with 8, 10, and 12 anchors in each track slab, the pattern of relative displacements in path A is similar to the track with 6 anchors in each track slab in Fig. 16(c), and therefore not depicted.

Table 1 shows the comparison of maximum vertical relative displacements (U_y) between the track slab labeled with 3 in Fig. 6 and the mortar layer with different combinations of anchors and coatings. It should be noted that the values in the table are the proportions of the maximum U_y for each scenario to the maximum U_y for the uncoated track with 0 anchors. Since the efficiency of different maintenance methods in mitigating damages for the continuous slab tracks has not been evaluated previously, this paper exhibits new findings that in comparison with the original track, the track with anchors, coatings, and combined use of both can reduce the maximum vertical relative displacement between the track slab and the mortar layer by 75%, 40% and 85% respectively.

Fig. 17 gives the interface damage variable at point A when the temperature is fully loaded. It can be found that the interface at point A is failed or severely damaged when there is no anchor. D can be slightly reduced when 4 anchors are installed in each track slab. And D turns to zero when there are 6 or more anchors in each track slab, whether coatings are applied or not. Interfacial failure at point A can lead to voids in the track structure which are difficult to detect and repair (Ma et al., 2020; Guo et al., 2021; Park et al., 2020; Zhu et al., 2019). Therefore, based on the above-mentioned finding, 6 or more anchors in each track slab are recommended to prevent such inner interface defects or voids.

Fig. 18 provides the interface damage variable at point B. It can be seen that D increases when anchors are used, and 6 or more anchors are generally better than 4 anchors in each track slab regarding lowering interface damage at point B. When there are 6 or more anchors, improvement of anchor quantity does not have a significant impact on

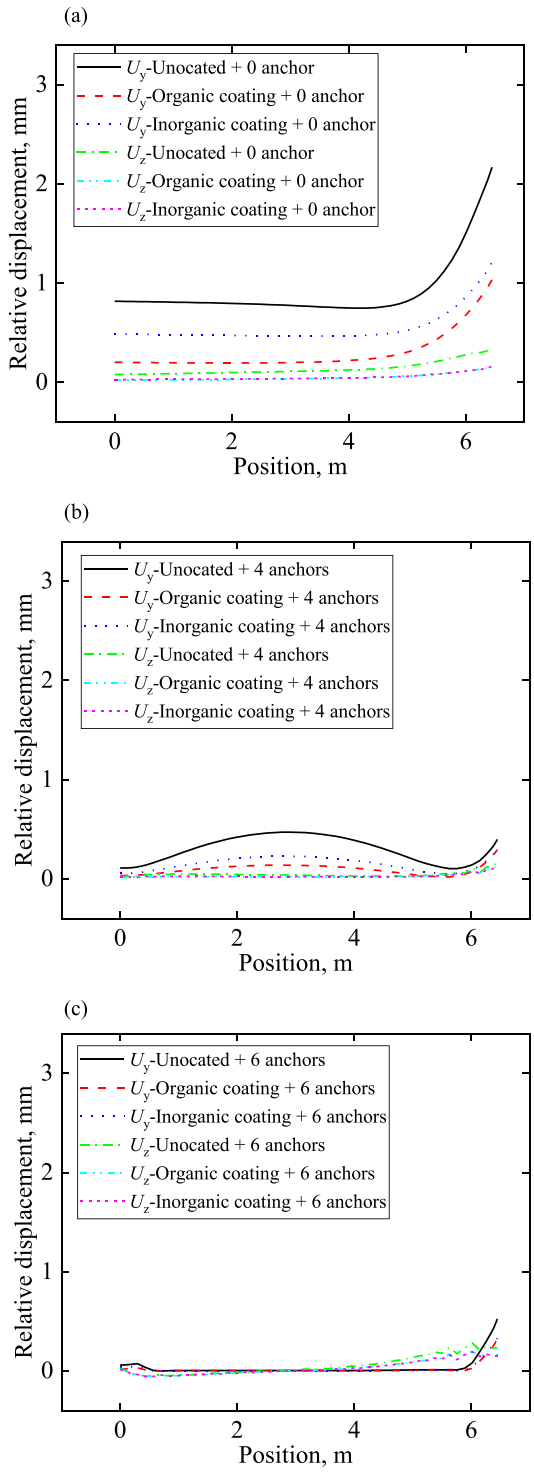

Fig. 16. Relative displacements between the track slab and the mortar layer in path A for the longitudinally continuous slab track with (a) 0 anchors, (b) 4 anchors, and (c) 6 anchors. Uy and Uz represent vertical relative displacement and longitudinal relative displacement respectively.

Table 1
Comparison of maximum U_y with different repairing methods.

	Uncoated	With organic coating	With inorganic coating
0 anchor	100.0%	47.7%	55.6%
4 anchors	21.7%	13.6%	13.7%
6 anchors	24.2%	14.8%	15.2%

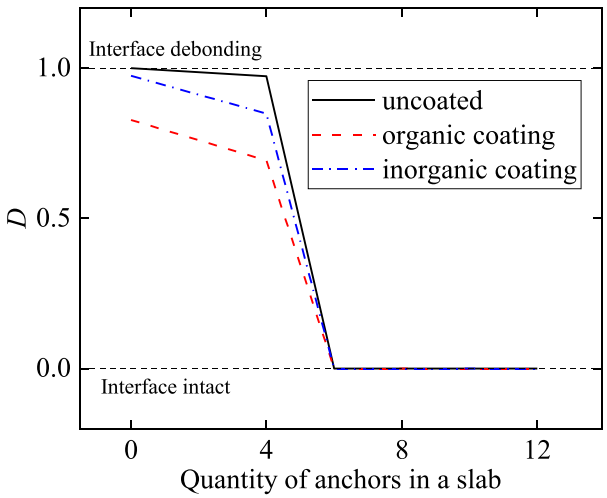

Fig. 17. Interface damage of the longitudinally continuous slab track with different quantities of anchors in a slab at point A.

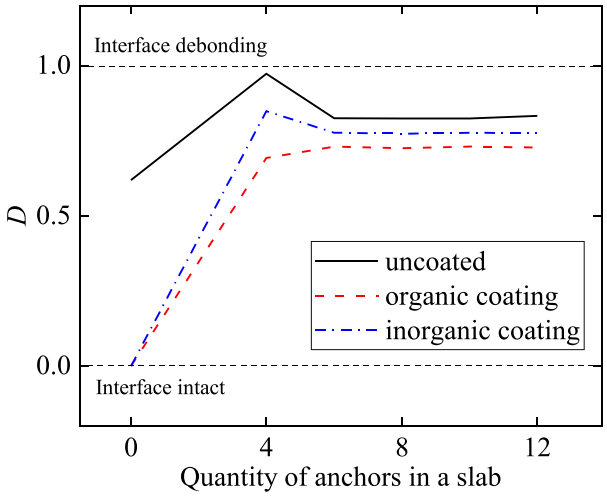

Fig. 18. Interface damage of the longitudinally continuous slab track with different quantities of anchors in a slab at point B.

the interface damage at both point A and point B. Therefore, from the perspective of economy, 6 anchors in each track slab can be a good choice. For the anchor-reinforced track, the organic coating outweighs the inorganic coating to improve the interface damage mitigation.

4.2. *Effect of repair methods on the slab end arching*

While ballasted tracks tend to buckle laterally when the temperature is high (Chayut et al., 2021; Fu et al., 2023; Amin et al., 2021), ends of track slabs neighboring damaged joints are likely to arch vertically when the track is subjected to temperature rise (Li et al., 2023; Cai et al., 2019). The anchors have been pulled out more from the concrete base than the track slabs since the bond strength between the anchors and the concrete base is lower than that for the track slabs. Fig. 19 reveals the development of the vertical displacement of the damaged joint for the track with organic coating. It can be found from Fig. 19(a) that the middle of the lateral path for the damaged joint rises under temperature rise when no anchor is used. Fig. 19(b) and (c) indicate that the arching in the middle of the lateral path is suppressed by the anchors. In addition, the vertical displacement increases nonlinearly with increasing temperature when there is no anchor, and goes up generally linearly with rising temperature when anchors are used. According to

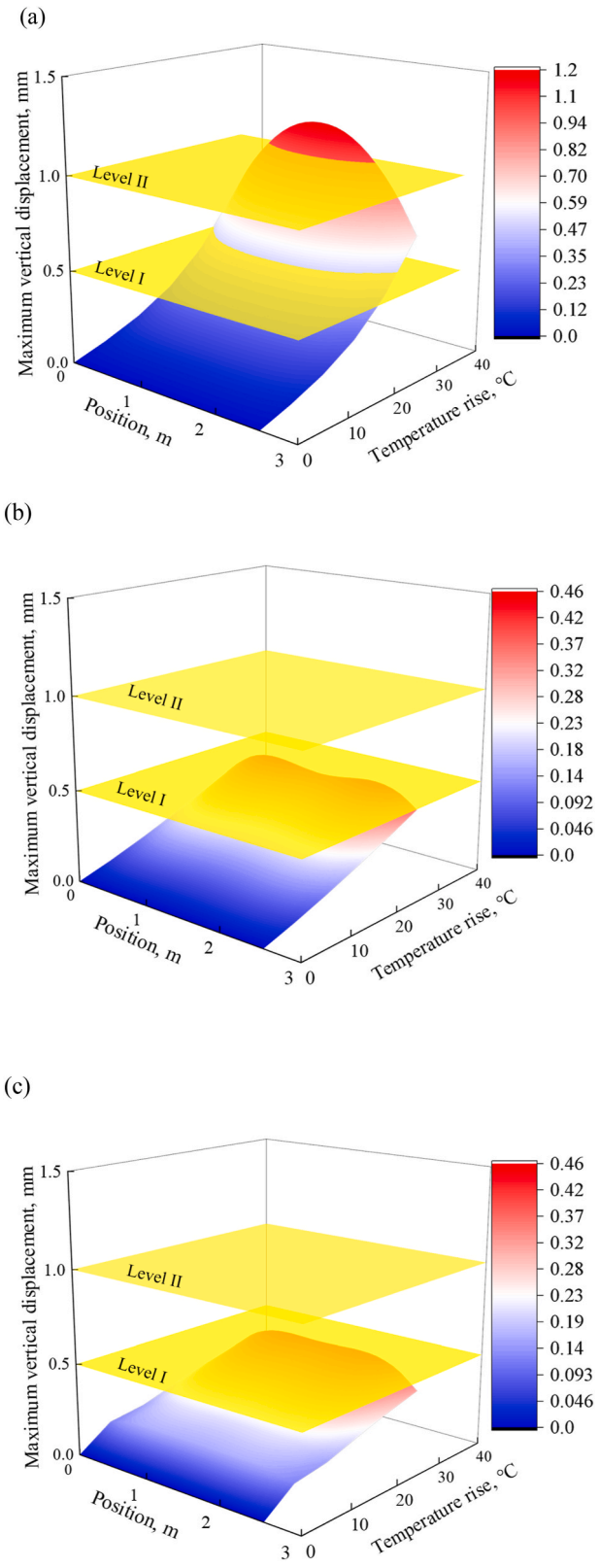

Fig. 19. Development of vertical displacement of the damaged joint for the longitudinally continuous slab track with the organic coating and (a) 0, (b) 4, (c) 6 anchors in each slab.

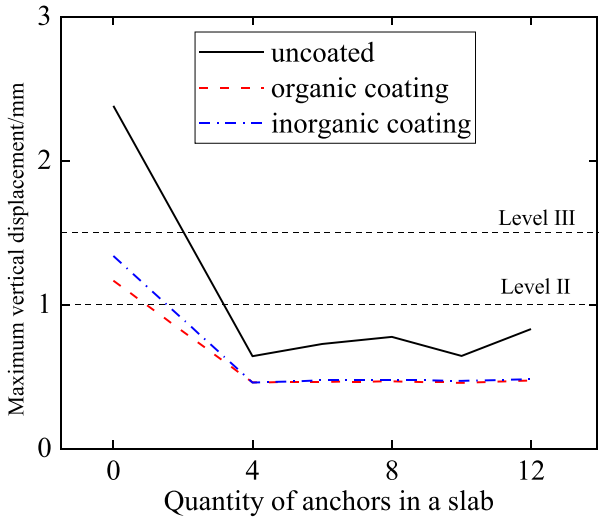

Fig. 20. Maximum vertical displacement of the damaged joint of the longitudinally continuous slab track with different quantities of anchors in a slab.

Maintenance Rules for Ballastless Track of High-speed Railway in China, interlayer gaps exceeding 0.5 mm, 1 mm, and 1.5 mm are defined as damages of Level I, Level II and Level III respectively. It can be known that there will be damages of level II when no anchor is used. However, when 4 or 6 anchors are used, there will be no damage of Level I.

The level of slab end arching can be represented by the maximum vertical displacement of the damaged joint, as shown in Fig. 20. It can be seen that for the track without anchors, the maximum vertical displacement of the damaged joint decreases by 51% and 44% when the organic coating and the inorganic coating are used respectively. When there are 4 or more anchors in each track slab, the maximum vertical displacement of the damaged joint for the coated tracks is between 60% and 73% of the uncoated track, no matter which coating is utilized. The maximum vertical displacement of the damaged joint stabilizes for the coated track with 4 or more anchors.

5. Conclusions

Temperature-induced damages such as interface debonding and slab end arching have become a critical issue for the longitudinally continuous slab tracks in practice. It is of great importance and necessity to assess the effects of the combined use of multiple maintenance methods and to evaluate the efficiency of different maintenance methods. In this paper, temperature-induced damages of the anchor-reinforced and coated longitudinally continuous slab tracks have been investigated. A novel finite element model of the longitudinally continuous slab track has been established and incorporated with a cohesive zone model to mimic the nonlinear constitution relationships. The effects of post-installed anchors and solar reflective coatings on the development of the interface damage and slab end arching have been systemically investigated. The following conclusions are drawn:

Interface damage between the track slabs and the mortar layer is mainly caused by the vertical relative displacement between the two layers.

This paper is the first to assess the influences of the combined use of multiple maintenance methods and to identify the effectiveness of different maintenance methods in mitigating track damages. It reveals that in comparison with the original track, the track with anchors, coatings, and combined use of both can reduce the maximum vertical relative displacement between the track slab and the mortar layer by 75%, 40%, and 85% respectively.

In comparison with 4 anchors, 6 or more anchors in each track slab can help to prevent inner interface defects. However, an increase in

anchor quantity above 6 anchors does not have a significant impact on the interface damage mitigation. Therefore, from the perspectives of both effectiveness and economy, 6 anchors in each track slab can be a good choice.

For the anchor-reinforced track, the organic coating outweighs the inorganic coating to improve interface damage mitigation.

When there are 4 or more anchors in each track slab, the maximum vertical displacement of the damaged joint for the coated track is between 60% and 73% of the uncoated track, no matter which coating is utilized.

It should be noted that although the mechanical behavior of reinforced and coated longitudinally continuous slab tracks installed on railway viaducts are studied, the drawn conclusions in this paper are also valid for the tracks installed on the subgrade because the structure of the tracks on railway viaducts is similar to that on the subgrade.

The short-term effects of temperature changes on the reinforced and coated slab track have been evaluated while the influences of repeated train loads have been neglected in this paper. The combine action of temperature changes and train loads will be investigated in future works.

Funding statement

The authors would like to acknowledge The National Key Research and Development Program of China (No. 2021YFB2601000), Natural Science Foundation of Hebei Province, China (No. E2021210142, E2022210086), Research and Development Project of Science and Technology of China State Railway Group Co., Ltd. (No. K2022G038), and the China Scholarship Council for the financial support. The authors are also grateful to European Commission for the support through Marie Curie RISEN project (Grant No 691135). The APC has been kindly sponsored by the University of Birmingham Library's Open Access Fund.

Declaration of competing interest

The authors declare that they have no known competing financial interests or personal relationships that could have appeared to influence the work reported in this paper.

Data availability

Data will be made available on request.

References

Amin, M., Manicka, D., David, T., et al., 2021. Analysis of Buckling Failure in Continuously Welded Railway Tracks. Engineering Failure Analysis, 104989.
Cai, X.P., Luo, B.C., Zhong, Y.L., et al., 2019. Arching mechanism of the slab joints in CRTSII slab track under high temperature conditions. Eng. Fail. Anal. 98, 95–108.
Cao, S.H., Yang, R.S., Su, C.G., et al., 2016. Damage Mechanism of Slab Track under the Coupling Effects of Train Load and Water [J]. Engineering Fracture Mechanics, pp. 160–175.
Chayut, N., Sakdirat, K., Charalampos, B., 2021. Nonlinear buckling instabilities of interspersed railway tracks. Comput. Struct. 106516. https://doi.org/10.1016/j.compstruc.2021.106516.
Chen, S.H., Mitsume, N., Bui, T.Q., et al., 2019a. Development of two intrinsic cohesive zone models for progressive interfacial cracking of laminated composites with matching and non-matching cohesive elements. Compos. Struct. 229, 111406.
Chen, S.H., Mitsume, N., Gao, W., et al., 2019b. A nodal-based extrinsic cohesive/contact model for interfacial debonding analyses in composite structures. Comput. Struct. 215, 80–97.
Chen, S.H., Chen, H., Mitsume, H., et al., 2021. A nodal-based Lagrange multiplier/cohesive zone approach for dynamic interfacial cracking analysis of thin-walled laminated composite structures. Compos. Struct. 256, 113112.
Choubane, B., Tia, M., 1992. Nonlinear temperature gradient effect on maximum warping stresses in rigid pavements. Transport. Res. Rec. 1370, 11–19.
Cui, S.L., Sun, X.G., Luan, M.S., et al., 2021. Research on Crack Detection Method of Ballastless Track Slab Based on Infrared Thermometer. Infrared Physics & Technology, 103772.
Dai, G.L., Li, M., 2016. Numerical Stimulation of interface delamination failure for prefabricated slab ballastless track. Journal of South China University of Technology:Natural Science Edition 44 (7), 102–122.
Dai, G.L., Su, M., 2016. Full-scale field experimental investigation on the interfacial shear capacity of continuous slab track structure. Arch. Civ. Mech. Eng. 16 (3), 485–493.
Deng, S.J., Ren, J.J., Wei, K., et al., 2021. Fatigue damage evolution analysis of the CA mortar of ballastless tracks via damage mechanics-finite element full-couple method. Construct. Build. Mater. 295, 123679.
Fu, H., Yang, Y., Kaewunruen, S., 2023. Multi-hazard effects of crosswinds on cascading failures of conventional and interspersed railway tracks exposed to ballast washaway and moving train loads. Sensors 23 (4), 1786. https://doi.org/10.3390/s23041786.
Gao, L., He, N., Ren, X.C., et al., 2020. Research on effect law of arch deformation of ballastless track slab. Huazhong Univ.of Sci.& Tech(Natural Science Edition) 48 (3), 92–97.
Gesualdo, A., Penta, F., 2018. A model for the mechanical behaviour of the railway track in the lateral plane. Int. J. Mech. Sci. 146, 303–318.
Guo, G.R., Wang, J.F., Du, B.W., et al., 2021. Application study on fiber optic monitoring and identification of CRTS-II-slab ballastless track debonding on viaduct. Appl. Sci. 11 (6239), 6239.
Heng, J., Zheng, K., Kaewunruen, S., Zhu, J., Baniotopoulos, C., 2020. Probabilistic fatigue assessment of rib-to-deck joints using thickened edge U-ribs. Steel Compos. Struct. 35 (6), 799–813. https://doi.org/10.12989/scs.2020.35.6.799.
Kaewunruen, S., Guo, Y., Jing, G., Matsumoto, A., 2023. Circular economy implementation in railway systems beyond net zero. Front. Built Environ. 9, 1239740. https://doi.org/10.3389/fbuil.2023.1239740.
Kaewunruen, S., Sussman, J., Einstein, H., 2016. Strategic framework to achieve carbon-efficient construction and maintenance of railway infrastructure systems. Front. Environ. Sci. 3 (3), 3. https://doi.org/10.3389/fenvs.2015.00006.
Kang, W.X., 2018. Applicability Analysis of the Solar Heat Reflective and Insulation Coating Used in the Ballastless Track. Master of thesis. Southwest Jiaotong University, Chengdu, China.
Kang, W.X., Chen, S., Wei, C.C., et al., 2019. Temperatures of ballastless track and effect of continuous hot weather. Journal of Railway 41 (7), 127–134.
Khajehdezfuly, A., Poorveis, D., Amiri, A.M., 2023. Effect of track flexibility on fatigue life of railway concrete slab track. Construct. Build. Mater. 382, 131341.
Li, Y., Chen, J.J., Wang, J.X., et al., 2020. Study on the interface damage of CRTS II slab track under temperature load. Structures 26, 224–236.
Li, Y., Chen, J.J., Wang, J.X., et al., 2021a. Interfacial failure and arching of the CRTS II slab track reinforced by post-installed reinforcement bars due to thermal effects. Eng. Fail. Anal. 125, 105405.
Li, Y., Chen, J.J., Jiang, Z.Q., et al., 2021b. Thermal performance of the solar reflective fluorocarbon coating and its effects on the mechanical behavior of the ballastless track. Construct. Build. Mater. 291, 123260.
Li, Y., Chen, J.J., Shi, X.F., et al., 2022a. Deformation and damage laws of CRTS II slab ballastless track reinforced by post-installed rebar subjected to high temperature load. China Railw. Sci. 43 (2), 19–27.
Li, Y., Chen, J.J., Wang, J.X., et al., 2022b. Study on the effects of solar reflective coatings on the interfacial damage of the CRTSII slab track. Construct. Build. Mater. 325, 126711.
Li, Y., Li, H.Y., Zhang, G.P., Kaewunruen, S., 2023. Nonlinear responses of longitudinally coupled slab tracks exposed to extreme heat waves. Eng. Struct. 281, 115789. https://doi.org/10.1016/j.engstruct.2023.115789.
Liang, R.H., Liu, W.F., Li, C.Y., et al., 2023. A novel efficient probabilistic prediction approach for train-induced ground vibrations based on transfer learning. J. Vib. Control. https://doi.org/10.1177/10775463221148792 online publication.
Liu, Y., Zhao, G.T., 2013. Analysis of early gap between layers of CRTSII slab ballastless track structure. China Railw. Sci. 34 (4), 1–7.
Liu, J., Zheng, X.G., Xie, Y.J., et al., 2011. Experimental study on grouting technology of cement emulsified asphalt mortar for CRTSII slab ballastless track. Construction Technology 40 (340), 49–52.
Lou, L.W., Xie, Y.J., Zheng, X.G., et al., 2015. Cause analysis and preventive measures on bubble of CRTSII cement emulsified asphalt mortar layer. Construction Technology 44 (4), 89–91.
Lu, Z.H., Wang, J., Tang, Z., et al., 2022. A novel cohesive zone model for predicting the interface bonding behaviour of the ballastless track of high-speed railway. Structures 41 (10), 1–14.
Lubliner, J., Oliver, J., Oller, S., et al., 1989. A plastic damage model for concrete. Int. J. Solid Struct. 25 (3), 299–326.
Ma, Z.R., Gao, L., Zhong, Y.L., et al., 2020. Arching detection method of slab track in high-speed railway based on track geometry data. Appl. Sci. 10 (6799), 6799.
Mahaboonpachai, T., Matsumoto, T., Inaba, Y., 2010. Investigation of interfacial fracture toughness between concrete and adhesive mortar in an external wall tile structure. Int. J. Adhesion Adhes. 30, 1–9.
Mao, X.J., 2020. Technology of replacing ballastless track slab by track shifting for high speed railway. Railw. Eng. 60 (5), 94–97.
Matias, S.R., Ferreira, P.A., 2022. The role of railway traffic and extreme weather on slab track long-term performance. Construct. Build. Mater. 322, 126445.
Ministry of Housing and Urban-Rural Development of the People's Republic of China, 2014. Code for Design of Concrete Structures, GB 50010−2010 [S]. China Construction Industry Press, Beijing, p. 211.
Ni, Y.F., Ren, J.J., Zhao, H.W., 2016. Study on anchoring scheme of lifted track slab in repairing of CRTS II slab-type ballastless track. Railw. Eng. (2), 132–135.
Park, S., Cho, H., Lim, Y., 2020. Nondestructive detection of gaps between railway track slabs and soil foundation using leaked air waves. Appl. Sci. 10 (3347), 3347.
Qi, S.X., Ren, J.J., Liu, X.Y., 2015. Influence of debonding on the performance of CRTSII slab track turnouts on large bridges. Eng. Mech. 32 (6), 124–132.
Ren, J.J., Wang, J., Li, J.L., et al., 2019. Damage law of track slab based on concrete damaged plasticity model. J. Zhejiang Univ. Eng. Sci. 53 (8), 1448–1456.

Rungskunroch, P., Shen, Z., Kaewunruen, S., 2021. Benchmarking environmental and economic impacts from the HSR networks considering life cycle perspectives. Environ. Impact Assess. Rev. 90, 106608. https://doi.org/10.1016/j.eiar.2021.106608.

Sresakoolchai, J., Kaewunruen, S., 2023. Interactive reinforcement learning innovation to reduce carbon emissions in railway infrastructure maintenance. Dev. Built. Environ. 15, 100193. https://doi.org/10.1016/j.dibe.2023.100193.

Tan, S.H., Fang, W.S., Lin, C., 2020. Stability analysis and maintenance suggestion of CRTSII Slab ballastless track. Railw. Eng. 60 (6), 136–139.

Tarifa, M., Zhang, X.X., Ruiz, G., et al., 2015. Full-scale fatigue tests of precast reinforced concrete slabs for railway tracks. Eng. Struct. 100, 610–621.

Wang, X.Y., Xia, L., 2012. Analysis of cause for quality problems of cement emulsified asphalt mortar and prevention. Journal of Railway Engineering Society (7), 57–61.

Wang, J.F., Zhou, Y.B., Wu, T.M., et al., 2019. Performance of cement asphalt mortar in ballastless slab track over high-speed railway under extreme climate conditions. Int. J. GeoMech. 19 (5), 04019037.

Xiao, H., Zhang, Y.R., Li, Q.H., et al., 2018. Analysis of the initiation and propagation of fatigue cracks in the CRTSII slab track inter-layer using FE-SAFE and XFEM. Proc IMechE Part F: Journal of Rail and Rapid Transit 6 (9), 1–13.

Xu, H., Liu, X., Xu, J.H., 2013. Influence on CRTSII slab track structure caused by the debonding between slab and CA mortar under the action of temperature load. Railway Standard Design (9), 9–12.

Xu, L., Yu, Z.W., Shan, Z., 2021. Numerical simulation for train–track–bridge dynamic interaction considering damage constitutive relation of concrete tracks. Arch. Civ. Mech. Eng. 21 (3), 116.

Xu, L., Liu, H.B., Yu, Z.W., 2022. A coupled model for investigating the interfacial and fatigue damage evolution of slab tracks in vehicle-track interaction. Appl. Math. Model. 772–790.

Yan, B., Liu, S., Dai, G.L., et al., 2016. Vertical nonlinear temperature distribution and temperature mode of unballasted track in typical areas of China. J. China Railw. Soc. 38 (8), 81–86.

Yang, J.J., Zhang, N., Gao, M.M., et al., 2016. Temperature warping and it's impact on train-track dynamic response of CRTSII ballastless track. Eng. Mech. 33 (4), 210–217.

Yang, X., Lin, S., Li, Y., et al., 2019. Can high-speed rail reduce environmental pollution? Evidence from China. J. Clean. Prod., 118135

Yang, Y., Zhang, G.J., Wu, G., et al., 2022. Study on fatigue damage laws and life prediction of CRTS-II ballastless track slab. Eng. Struct. 295, 113659.

Ye, W.L., Deng, S.J., Ren, J.J., et al., 2022. Deep learning-based fast detection of apparent concrete crack in slab tracks with dilated convolution. Construct. Build. Mater. 329, 127157.

Yi, Z., Li, H., Wen, H., et al., 2015. Study on remedy technology of open joint of filling layer for CRTS II slab-type ballastless track. Railw. Eng. 55, 102–106.

Zhang, J.W., Jiang, H.L., Ding, F., et al., 2020. Effects of metal-ceramic anticorrosion coating on the performance of ballastless tracks at high temperature. Arch. Civ. Mech. Eng. 20 (4), 120.

Zhang, Q., Cai, X., Zhong, Y., et al., 2022. Temperature field and thermal effects of the longitudinal connected slab track based on the measurement data and thermal-fluid-structure coupling analysis. Construct. Build. Mater. 343, 128121.

Zhao, H., 2017. High Temperature deformation and damage mechanism of CRTSII ballastless slab track on high speed tailway. Railway Standard Design 61 (9), 46–50.

Zhao, G.T., Liu, Y., 2020. Mechanism analysis of delamination of CRTSIIslab ballastless track structure. J. China Railw. Soc. 42 (7), 117–126.

Zhao, H., Li, Q.Y., Huang, C.Y., et al., 2021. Preventive reinforcement scheme and application of CRTSII SlabBallastless track for high speed railway. Railw. Eng. 61 (4), 116–119.

Zhong, L.Y., Gao, L., Wang, P., et al., 2018. Mechanism of interfacial shear failure between CRTSII slab and CA mortar under temperature loading. Eng. Mech. 35 (2), 230–238.

Zhou, R., Zhu, X., Ren, W.X., et al., 2022. Thermal evolution of CRTS II slab track under various environmental temperatures: experimental study. Construct. Build. Mater. 325, 126699.

Zhou, R., Yue, H.H., Du, Y.L., et al., 2023a. Experimental and numerical study on interfacial thermal behavior of CRTS II slab track under continuous high temperatures. Eng. Struct. 284, 115964.

Zhou, R., Zhu, X., Du, Y.L., et al., 2023b. Thermal response of the bridge supported longitudinal CRTS II slab track subject to diurnal temperature variation. Construct. Build. Mater. 395, 132332.

Zhou, R., Yuan, W.H., Liu, W.B., et al., 2023c. Thermal performance of CRTS II slab track-bridge structure under extreme temperatures: numerical simulation. Construct. Build. Mater. 377, 131147.

Zhu, S.Y., Cai, C.B., 2014. Interface damage and its effect on vibrations of slab track under temperature and vehicle dynamic loads. Int. J. Non Lin. Mech. 58, 222–232.

Zhu, W.F., Chen, X.J., Li, Z.W., et al., 2019. A SAFT method for the detection of void defect inside a ballastless track structure using ultrasonic array sensors. Sensors 19, 4677.